Stochastic reduced-order model for the dynamical analysis of complex structures with a high modal density

O. Ezvan, Anas Batou, Christian Soize

Stochastic reduced-order model for the dynamical analysis of complex structures with a high modal density

O. Ezvan [1], **A. Batou** [1], **C. Soize** [1]
[1] Université Paris-Est, Modélisation et Simulation Multi-Echelle, MSME UMR 8208 CNRS,
5 Boulevard Descartes, 77454 Marne-la-Vallée, France
e-mail: **olivier.ezvan@u-pem.fr**

In the proceedings of the international conference USD 2014, Katholieke Universiteit Leuven, Belgium, September 15-17, 2014

Abstract

In this research, we are interested in predicting the dynamical response of complex structures characterized by the presence of numerous local elastic modes that appear immediatly in the low-frequency range. Where the modal analysis method would classically provide a small-dimension basis constituted of global displacements for the construction of a robust and accurate reduced-order model adapted to the case of a low modal density, it is not the case considered here. Unlike global displacements, the local displacements are very sensitive to both parameters uncertainties and model uncertainties induced by modeling errors. This paper presents an original methodology which allows us to separate the admissible displacements space into the two algebraically independent subspaces of global and local displacements. This global/local separation allows a separated nonparametric probabilistic model of uncertainties to be implemented and thus allows the variabilities of the global displacements and of the local displacements to be controlled separately.

1 Introduction

In general, the low-frequency range is characterized by the presence of a few well-separated resonances associated with global elastic modes corresponding to large-wavelength vibrations [1]. In contrast, the high-frequency regime is characterized by a smooth frequency response associated with a high modal density constituted of small-wavelength vibrations modes. These local elastic modes are very sensitive to both modelisation errors and system-parameters uncertainties. The medium-frequency band constituted of both global modes and numerous local elastic modes is thus also very sensitive to uncertainties introduced in the computational model. The modal analysis method [2, 1] then allows the construction of an accurate and robust small-dimension reduced-order model adapted to the low-frequency range whereas Statistical Energy Analysis (SEA, see [3, 4]) is adapted to the high-frequency band.

Beyond the first resonances, the model uncertainties associated with the modeling errors, the system-parameters uncertainties, and the manufacturing variabilities make the use of a deterministic model not robust and thus not sufficiently predictive. The parametric probabilistic approach of uncertainties [5, 6] allows the system-parameters uncertainties to be addressed. The nonparametric probabilistic approach allows the modeling errors to be taken into account [7]. Both the system-parameters uncertainties and the modeling errors can be modeled using a generalized approach [8].

In this research, we are interested in predicting the dynamical response of complex structures in a broad frequency band that includes the low-frequency band, and for which their increasingly detailed finite element

models yield an emergence of numerous elastic modes immediately in the low-frequency range, captured with the modal analysis method. We consider structures made up of a stiff master structure supporting flexible components, which are responsible for the occurrence of such local elastic modes among the usual global elastic modes. A recent methodology has been developed [9, 10], which consists in splitting the admissible displacements space into two independent admissible displacements subspaces defined as the global displacements space and the local displacements space. The introduction of such global and local coordinates allows us to adapt the model of uncertainties to each type of coordinates. The bases associated with these two spaces are not constituted of usual elastic modes since the latter cannot always be defined either as global or as local elastic modes. Indeed, an elastic mode is, in general, a combination of global and local displacements contributions. These unusual bases are constructed solving generalized eigenvalue problems for which the kinetic energy is modified (kinematics reduction) while the elastic energy is kept exact. More precisely, such a kinematics reduction associated with the mass matrix allows local elastic modes to be filtered. In this paper, we present an extension of this methodology consisting in splitting the admissible displacements space into several admissible displacements subspaces that correspond to the different spatial scales of the structure. This way, the model of uncertainties can then be adapted to each scale.
The theoretical dethronements relative to this multiple separation are presented considering three spatial scales denoted as $\mathcal{L}$, $\mathcal{M}$, and $\mathcal{H}$, respectively associated with the low-frequency (LF), medium-frequency (MF), and high-frequency (HF) bands. A numerical application is then presented for a heterogeneous thin plate constituted of three structural scales.

2 Nominal computational dynamical model

We are interested in predicting, within the frequency band of analysis $\mathcal{B} = [\omega_{\min}, \omega_{\max}]$, the dynamical response of a tridimensional linear damped structure occupying a bounded domain Ω , fixed on a part of its boundary and subjected to external loads on the other part. The nominal computational dynamical model is constructed using the finite element method [11, 12]. For all ω in $\mathcal{B}$, the complex vector $\mathbb{U}(\omega)$ of the m degrees of freedom is the solution of the following matrix equation,

$$(-\omega^2 [\mathbb{M}] + i\omega [\mathbb{D}] + [\mathbb{K}])\mathbb{U}(\omega) = \mathbb{F}(\omega) , \tag{1}$$

where $[\mathbb{M}]$, $[\mathbb{D}]$, and $[\mathbb{K}]$ are the symmetric positive-definite $(m \times m)$ real mass, damping and stiffness matrices, and where $\mathbb{F}(\omega)$ is the complex vector associated with the external forces.

3 Modal analysis method

As it is well known [1, 2], the eigenfrequencies ω_α and the associated elastic modes $\boldsymbol{\varphi}_\alpha$ in $\mathbb{R}^m$ are obtained solving the generalized eigenvalue problem associated with the conservative dynamical system,

$$[\mathbb{K}]\, \boldsymbol{\varphi}_\alpha = \lambda_\alpha\, [\mathbb{M}]\, \boldsymbol{\varphi}_\alpha , \tag{2}$$

where the real eigenvalues $\lambda_\alpha = \omega_\alpha^2$ are such that $0 < \lambda_1 \leq \lambda_2 \leq \ldots \leq \lambda_m$. The elastic modes form a vector basis of $\mathbb{R}^m$, and the modal analysis method consists in approximating vector $\mathbb{U}(\omega) \in \mathbb{C}^m$ in the subspace spanned by the first n elastic modes ($n \ll m$), such that

$$\forall \omega \in \mathcal{B}, \quad \mathbb{U}(\omega) \simeq \mathbb{U}_n(\omega) = \sum_{\alpha=1}^{n} q_\alpha(\omega) \boldsymbol{\varphi}_\alpha = [\Phi]\ \boldsymbol{q}(\omega) , \tag{3}$$

where $[\Phi] = [\boldsymbol{\varphi}_1 \ldots \boldsymbol{\varphi}_n]$ is the $(m \times n)$ real matrix constituted of the first n elastic modes (associated with the n smallest eigenvalues), and where the complex vector $\boldsymbol{q}(\omega)$ in $\mathbb{C}^n$ of the generalized coordinates is obtained solving, for all ω in $\mathcal{B}$,

$$(-\omega^2 [M] + i\omega [D] + [K])\, \boldsymbol{q}(\omega) = \boldsymbol{\mathcal{F}}(\omega) , \tag{4}$$

where $[M] = [\Phi]^T [\mathbb{M}] [\Phi]$, $[D] = [\Phi]^T [\mathbb{D}] [\Phi]$, and $[K] = [\Phi]^T [\mathbb{K}] [\Phi]$ are the symmetric positive-definite $(n \times n)$ real generalized mass, damping and stiffness matrices, and where $\boldsymbol{\mathcal{F}}(\omega) = [\Phi]^T \mathbb{F}(\omega)$ is the generalized force. The modal contributions of elastic modes associated with higher eigenfrequencies are thus neglected.

4 Frequency-multiscale decomposition of the admissible displacements space

4.1 Kinematics decomposition for the kinetic energy

Let $\mathbb{H}_r^1$ be a subspace of $\mathbb{R}^m$ of dimension d_r^1 and let, for $\mathbb{U}$ in $\mathbb{R}^m$, the vector $\mathbb{U}_1^r$ be the orthogonal projection of $\mathbb{U}$ on $\mathbb{H}_r^1$ with respect to the $\mathbb{M}$-inner product defined as $\langle \mathbf{v}, \mathbf{w} \rangle_{\mathbb{M}} = \mathbf{w}^T [\mathbb{M}] \mathbf{v}$, for $\mathbf{v}$ and $\mathbf{w}$ in $\mathbb{R}^m$. The projection matrix $[H_1^r]$ of rank d_r^1 is such that $\mathbb{U}_1^r = [H_1^r]\mathbb{U}$. The residual $\mathbb{U}_1^c = \mathbb{U} - \mathbb{U}_1^r$, verifying the orthogonality property $(\mathbb{U}_1^c)^T [\mathbb{M}] \mathbb{U}_1^r = 0$, belongs to the complementary space denoted $\mathbb{H}_c^1$, image of the projection matrix $[H_1^c] = [I_m] - [H_1^r]$ of rank $d_c^1 = m - d_r^1$, such that $\mathbb{R}^m = \mathbb{H}_r^1 \oplus \mathbb{H}_c^1$.

Similarly, suppose $\mathbb{H}_r^2$ be a subspace of $\mathbb{R}^m$ of dimension $d_r^2 > d_r^1$ verifying $\mathbb{H}_r^2 \supset \mathbb{H}_r^1$ and let, for $\mathbb{U}$ in $\mathbb{R}^m$, the vector $\mathbb{U}_2^r$ be the orthogonal projection of $\mathbb{U}$ on $\mathbb{H}_r^2$ with respect to the $\mathbb{M}$-inner product. The projection matrix $[H_2^r]$ of rank d_r^2 is such that $\mathbb{U}_2^r = [H_2^r]\mathbb{U}$ and the residual $\mathbb{U}_2^c = \mathbb{U} - \mathbb{U}_2^r$ belongs to the complementary space denoted $\mathbb{H}_c^2$, image of the projection matrix $[H_2^c] = [I_m] - [H_2^r]$ of rank $d_c^2 = m - d_r^2$, such that $\mathbb{R}^m = \mathbb{H}_r^2 \oplus \mathbb{H}_c^2$.

We now introduce the three subspaces $\mathbb{H}_{\mathcal{L}}$, $\mathbb{H}_{\mathcal{M}}$, and $\mathbb{H}_{\mathcal{H}}$ of $\mathbb{R}^m$, associated with the three spatial scales $\mathcal{L}$, $\mathcal{M}$, and $\mathcal{H}$ for which we aim to separate the displacements. Let $\mathbb{H}_{\mathcal{L}}$ be such that $\mathbb{H}_{\mathcal{L}} = \mathbb{H}_r^1$, $\mathbb{H}_{\mathcal{H}}$ be such that $\mathbb{H}_{\mathcal{H}} = \mathbb{H}_c^2$, and $\mathbb{H}_{\mathcal{M}}$ be such that $\mathbb{H}_{\mathcal{M}} = \mathbb{H}_r^2 \cap \mathbb{H}_c^1$. As a consequence, space $\mathbb{H}_{\mathcal{L}}$ is the image of the projection matrix $[H^{\mathcal{L}}] = [H_1^r]$ of rank $d_{\mathcal{L}} = d_r^1$, space $\mathbb{H}_{\mathcal{H}}$ is the image of the projection matrix $[H^{\mathcal{H}}] = [H_2^c]$ of rank $d_{\mathcal{H}} = d_c^2$, and space $\mathbb{H}_{\mathcal{M}}$ is the image of the projection matrix $[H^{\mathcal{M}}] = [H_2^r] - [H_1^r]$ of rank $d_{\mathcal{M}} = d_r^2 - d_r^1$. It can be shown that these subspaces are independant and that their union is $\mathbb{R}^m$, i.e.

$$\mathbb{R}^m = \mathbb{H}_{\mathcal{L}} \oplus \mathbb{H}_{\mathcal{M}} \oplus \mathbb{H}_{\mathcal{H}} \,. \tag{5}$$

This decomposition will be used to restrict the displacement-vectors space for the kinetic energy to appropriate subspaces such that the displacements be spatially filtered for each scale.

4.2 Decomposition of the admissible displacements space and construction of the associated vector bases

Let $\mathcal{S}$ be $\mathcal{L}$, $\mathcal{M}$, or $\mathcal{H}$. The generalized eigenvalue problem associated with the conservative $\mathcal{S}$-scale dynamical system is defined as

$$[\mathbb{K}] \boldsymbol{\varphi}_\beta^{\mathcal{S}} = \lambda_\beta^{\mathcal{S}} [\mathbb{M}^{\mathcal{S}}] \boldsymbol{\varphi}_\beta^{\mathcal{S}} \,, \tag{6}$$

where the positive-semidefinite matrix $[\mathbb{M}^{\mathcal{S}}]$ of rank $d_{\mathcal{S}}$ is the $\mathcal{S}$-scale modified mass matrix, for which the associated kinetic energy is built upon displacements vectors that are restricted to the $\mathcal{S}$-scale displacements space $\mathbb{H}_{\mathcal{S}}$, and which is constructed as

$$[\mathbb{M}^{\mathcal{S}}] = [H^{\mathcal{S}}]^T [\mathbb{M}] [H^{\mathcal{S}}] \,, \tag{7}$$

such that the $d_{\mathcal{S}}$ $\mathcal{S}$-scale real eigenvectors $\left\{ \boldsymbol{\varphi}_\beta^{\mathcal{S}} \,, \beta = 1, \ldots, d_{\mathcal{S}} \right\}$ associated with the $d_{\mathcal{S}}$ finite positive eigenvalues $0 < \lambda_1^{\mathcal{S}} \leq \lambda_2^{\mathcal{S}} \leq \ldots \leq \lambda_{d_{\mathcal{S}}}^{\mathcal{S}}$ allow the $\mathcal{S}$-scale admissible displacements space, $\mathbb{V}_{\mathcal{S}}$, to be spanned.

We denote as $[\Phi^{\mathcal{S}}]$ the $(m \times n_{\mathcal{S}})$ real matrix constituted of the first $n_{\mathcal{S}}$ $\mathcal{S}$-scale eigenvectors such that $[\Phi^{\mathcal{S}}] = [\boldsymbol{\varphi}_1^{\mathcal{S}} \ldots \boldsymbol{\varphi}_{n_{\mathcal{S}}}^{\mathcal{S}}]$ with $n_{\mathcal{S}} \leq d_{\mathcal{S}}$. The $\mathcal{S}$-scale elastic modes $\boldsymbol{\psi}^{\mathcal{S}}$ are then defined as

$$\boldsymbol{\psi}^{\mathcal{S}} = [\Phi^{\mathcal{S}}]\widetilde{\boldsymbol{\psi}}^{\mathcal{S}} \,, \tag{8}$$

where the generalized $\mathcal{S}$-scale elastic modes $\widetilde{\boldsymbol{\psi}}^{\mathcal{S}}$ are the solutions of the generalized eigenvalue problem

$$[K^{\mathcal{S}\mathcal{S}}]\widetilde{\boldsymbol{\psi}}^{\mathcal{S}} = \mu^{\mathcal{S}}[M^{\mathcal{S}\mathcal{S}}]\widetilde{\boldsymbol{\psi}}^{\mathcal{S}} \,, \tag{9}$$

in which $[K^{\mathcal{S}\mathcal{S}}] = [\Phi^{\mathcal{S}}]^T[\mathbb{K}][\Phi^{\mathcal{S}}]$ and $[M^{\mathcal{S}\mathcal{S}}] = [\Phi^{\mathcal{S}}]^T[\mathbb{M}][\Phi^{\mathcal{S}}]$ are symmetric positive-definite $(n_{\mathcal{S}} \times n_{\mathcal{S}})$ real matrices. The $\mathcal{S}$-scale eigenfrequencies $\omega^{\mathcal{S}}$ are such that $\omega^{\mathcal{S}} = \sqrt{\mu^{\mathcal{S}}}$ and the $\mathcal{S}$-scale elastic modes $\boldsymbol{\psi}^{\mathcal{S}}$ are obtained using Eq. (8). The $(m \times n_{\mathcal{S}})$ real matrix $[\Psi^{\mathcal{S}}]$ constituted of the $n_{\mathcal{S}}$ $\mathcal{S}$-scale elastic modes is such that $[\Psi^{\mathcal{S}}] = [\boldsymbol{\psi}_1^{\mathcal{S}} \ldots \boldsymbol{\psi}_{n_{\mathcal{S}}}^{\mathcal{S}}]$ and is a vector basis of a subspace $\mathbb{V}_{\mathcal{S}}^{(n_{\mathcal{S}})}$ of $\mathbb{V}_{\mathcal{S}}$.
The construction of the $\mathcal{L}$-, $\mathcal{M}$-, and $\mathcal{H}$-scale displacements spaces $\mathbb{H}_{\mathcal{L}}$, $\mathbb{H}_{\mathcal{M}}$, and $\mathbb{H}_{\mathcal{H}}$ defined in Section 4.1 assures the $\mathcal{L}$-, $\mathcal{M}$-, and $\mathcal{H}$-scale admissible displacements spaces $\mathbb{V}_{\mathcal{L}}$, $\mathbb{V}_{\mathcal{M}}$, and $\mathbb{V}_{\mathcal{H}}$ to be such that

$$\mathbb{R}^m = \mathbb{V}_{\mathcal{L}} \oplus \mathbb{V}_{\mathcal{M}} \oplus \mathbb{V}_{\mathcal{H}} \,. \tag{10}$$

5 Reduced-order models

5.1 Nominal reduced-order model

Let $[\Psi] = [\Psi^{\mathcal{L}}\ \Psi^{\mathcal{M}}\ \Psi^{\mathcal{H}}]$ be the $(m \times n_t)$ real matrix constituted of the $\mathcal{L}$-, $\mathcal{M}$-, and $\mathcal{H}$-scale elastic modes, with $n_t = n_{\mathcal{L}} + n_{\mathcal{M}} + n_{\mathcal{H}}$. For all ω in $\mathcal{B}$, the generalized coordinates $\mathbf{q}(\omega)$ in $\mathbb{C}^{n_t}$ associated with the nominal reduced-order model are the solutions of the following matrix equation,

$$(-\omega^2[\underline{M}] + i\omega[\underline{D}] + [\underline{K}])\,\mathbf{q}\,(\omega) = \mathbf{F}\,(\omega) \,, \tag{11}$$

where $[\underline{M}] = [\Psi]^T[\mathbb{M}][\Psi]$, $[\underline{D}] = [\Psi]^T[\mathbb{D}][\Psi]$ and $[\underline{K}] = [\Psi]^T[\mathbb{K}][\Psi]$ are the symmetric positive-definite $(n_t \times n_t)$ real generalized mass, damping and stiffness matrices, and where $\mathbf{F}(\omega) = [\Psi]^T\mathbb{F}(\omega)$ is the generalized force. For all ω in $\mathcal{B}$, the approximation $\mathbb{U}_{n_{\mathcal{L}},n_{\mathcal{M}},n_{\mathcal{H}}}(\omega)$ of $\mathbb{U}(\omega)$ at order $(n_{\mathcal{L}}, n_{\mathcal{M}}, n_{\mathcal{H}})$ with $n_{\mathcal{L}} \leq d_{\mathcal{L}}$, $n_{\mathcal{M}} \leq d_{\mathcal{M}}$, and $n_{\mathcal{H}} \leq d_{\mathcal{H}}$ is then such that

$$\mathbb{U}(\omega) \simeq \mathbb{U}_{n_{\mathcal{L}},n_{\mathcal{M}},n_{\mathcal{H}}}(\omega) = \sum_{\beta=1}^{n_t} \mathrm{q}_\beta(\omega)\boldsymbol{\psi}_\beta = [\Psi]\,\mathbf{q}(\omega) \,, \tag{12}$$

in which $\boldsymbol{\psi}_\beta$ is the β-th column of matrix $[\Psi]$.

5.2 Stochastic reduced-order model

The nonparametric probabilistic approach [7] is used for modeling the uncertainties introduced in the reduced-order computational model, which are due to modeling errors, system-parameters uncertainties, and manufacturing variabilities.
In this section, letter A is used for M, D, or K.

5.2.1 Scale-independent probabilistic model of uncertainties

In the nonparametric probabilistic approach of uncertainties, matrix $[\underline{A}]$ is replaced by a random matrix $[\mathbf{A}]$ for which the probability distribution has been constructed [7] using the Maximum Entropy Principle [13, 14] with the following available information:

- Matrix $[\mathbf{A}]$ is with values in the set of all the symmetric positive-definite $(n_t \times n_t)$ real matrices.
- $E\{[\mathbf{A}]\} = [\underline{A}]$, where E is the mathematical expectation (which means that the mean value is chosen as the value of the nominal model).
- $E\{|||[\mathbf{A}]^{-1}||_F^2\} < +\infty$, where $||.||_F$ denotes the Frobenius norm.

As a result, matrix $[\mathbf{A}]$ is written as $[\mathbf{A}] = [\mathbf{L}(\delta^{\mathbf{A}})\ L_{\underline{A}}]^T [\mathbf{L}(\delta^{\mathbf{A}})\ L_{\underline{A}}]$, in which $[L_{\underline{A}}]$ is the upper triangular matrix given by the Cholesky factorization of $[\underline{A}]$ such that $[\underline{A}] = [L_{\underline{A}}]^T [L_{\underline{A}}]$, and where $[\mathbf{L}(\delta^{\mathbf{A}})]$ is a random upper triangular $(n_t \times n_t)$ real matrix defined in [7], and where $\delta^{\mathbf{A}}$ is the hyperparameter defined by

$$\delta^{\mathbf{A}} = \frac{E\{|||[\mathbf{A}] - [\underline{A}]||_F^2\}}{|||[\underline{A}]||_F^2} \quad , \tag{13}$$

which allows the level of uncertainties to be controlled.

5.2.2 Scale-dependent probabilistic model of uncertainties

The decomposition explicited in Section 4.2 of the admissible displacements space into several subspaces, each one of them corresponding to the admissible displacements space related to a given scale $\mathcal{S}$ ($\mathcal{L}$, $\mathcal{M}$, or $\mathcal{H}$), allows the level of uncertainties to be separately defined for each scale. Let $[P^{\mathcal{S}}]$ be the $(n_t \times n_{\mathcal{S}})$ matrix that allows the extraction of the sub-matrix in $[\underline{A}]$ related to the $\mathcal{S}$-scale basis coordinates. The random matrix $[\mathbf{A}]$ is then defined as

$$[\mathbf{A}] = [\mathbf{L}_{\mathbf{A}}]^T [\mathbf{L}_{\mathbf{A}}] \, , \tag{14}$$

in which the upper triangular $(n_t \times n_t)$ real random matrix $[\mathbf{L}_{\mathbf{A}}]$ is such that

$$[\mathbf{L}_{\mathbf{A}}] = \left[\ [\mathbf{P}_{\underline{A}}^{\mathcal{L}}] \quad [\mathbf{P}_{\underline{A}}^{\mathcal{M}}] \quad [\mathbf{P}_{\underline{A}}^{\mathcal{H}}] \ \right] \, , \tag{15}$$

where the $(n_t \times n_{\mathcal{S}})$ real random matrices $[\mathbf{P}_{\underline{A}}^{\mathcal{S}}]$, with $\mathcal{S}$ used for $\mathcal{L}$, $\mathcal{M}$, or $\mathcal{H}$, are defined by

$$[\mathbf{P}_{\underline{A}}^{\mathcal{S}}] = [\mathbf{L}(\delta_{\mathcal{S}}^{\mathbf{A}})] \ [L_{\underline{A}}] \ [P^{\mathcal{S}}] \, , \tag{16}$$

with $\delta_S^{\mathbf{A}}$ the hyperparameter controlling the level of uncertainties of the S-scale coordinates.

5.2.3 Stochastic reduced-order model

For all ω in $\mathcal{B}$, the random generalized coordinates $\mathbf{Q}(\omega)$ in $\mathbb{C}^{n_t}$ associated with the stochastic reduced-order model are solved, using the Monte-Carlo simulation method [15],

$$(-\omega^2 [\mathbf{M}] + i\omega [\mathbf{D}] + [\mathbf{K}]) \, \mathbf{Q}(\omega) = \mathbf{F}(\omega) \, , \tag{17}$$

where the symmetric positive-definite real random mass, damping and stiffness matrices $[\mathbf{M}]$, $[\mathbf{D}]$, and $[\mathbf{K}]$ are defined by Eq. (14). Then, for all ω in $\mathcal{B}$, the random response $\mathbf{U}_{n_{\mathcal{L}}, n_{\mathcal{M}}, n_{\mathcal{H}}}(\omega)$ is written as

$$\mathbf{U}_{n_{\mathcal{L}}, n_{\mathcal{M}}, n_{\mathcal{H}}}(\omega) = \sum_{\beta=1}^{n_t} Q_\beta(\omega) \boldsymbol{\psi}_\beta = [\Psi] \, \mathbf{Q}(\omega) \, , \tag{18}$$

and allows statistics such as the mean values and the confidence regions to be constructed.

6 Numerical application

6.1 Nominal computational dynamical model

The dynamical system (see Fig. 1) is a heterogenous $0.26 \times 0.2\, m^2$ plate constituted of a stiff master part and of 12 flexible panels that each support 4 highly-flexible sub-panels.

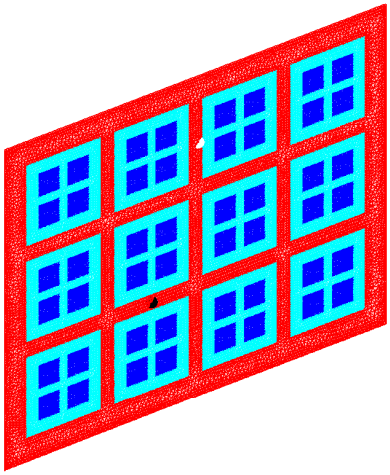

Figure 1: Dynamical System

The master structure (or the master frame, see Fig. 1, in red or in medium grey in b&w) is constituted of isotropic and homogeneous identical plates with width $0.01\, m$ or $0.015\, m$ (for the plates located at the edges), with Young modulus $210 \times 10^9\, Pa$, and with constant thickness $0.001\, m$. Each flexible panel (see Fig. 1, in light blue or in light grey in b&w) is constituted of isotropic and homogeneous identical plates with width $0.005\, m$ or $0.0075\, m$ at the common edges with the master structure, with Young moduli that are lightly different for each panel and with values around $210 \times 10^9\, Pa$, and with different constant thicknesses around $10^{-4}\, m$. The highly-flexible sub-panels (see Fig. 1, in dark blue or in dark grey in b&w) are isotropic and homogeneous square plates with side $0.015\, m$, with Young moduli that are lightly different for each sub-panel and with values around $210 \times 10^9\, Pa$, and with different constant thicknesses around $10^{-5}\, m$. These small variations are introduced so that the flexible panels and sub-panels vibration modes occur at distinct eigenfrequencies.

The master structure is modeled with about $14,500$ Kirchhoff plate elements, each flexible panel is modeled with about $2,700$ Kirchhoff plate elements, and each highly-flexible sub-panel is modeled with 550 Kirchhoff plate elements, with a total of about $73,000$ elements for the whole structure. As boundary conditions, the four corner nodes are fixed. The structure has $28,624$ nodes and $m = 85,860$ degrees of freedom. The frequency band of analysis is $\mathcal{B} = 2\pi \times]0, 1500]\, rad/s$.

6.2 Reduced-order models

6.2.1 Elastic modes

The elastic modes are computed using Eq. (2). In the frequency band of analysis $\mathcal{B}$, there are 410 elastic modes. The modal density is plotted in Fig. (2). In low frequency the modal density is low, whereas starting from around $1000 Hz$ the modal density is high and uniform in frequency.

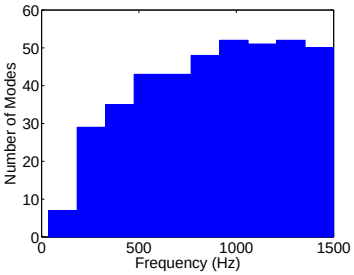

Figure 2: Modal density

The flexible panels are responsible for the presence of numerous local elastic modes and the proportion of global elastic modes rapidly decreases with respect to the frequency. A few elastic-mode shapes are shown in Fig. 3 and 4 to illustrate what is intended by $\mathcal{L}$-, $\mathcal{M}$-, and $\mathcal{H}$-scale displacements.

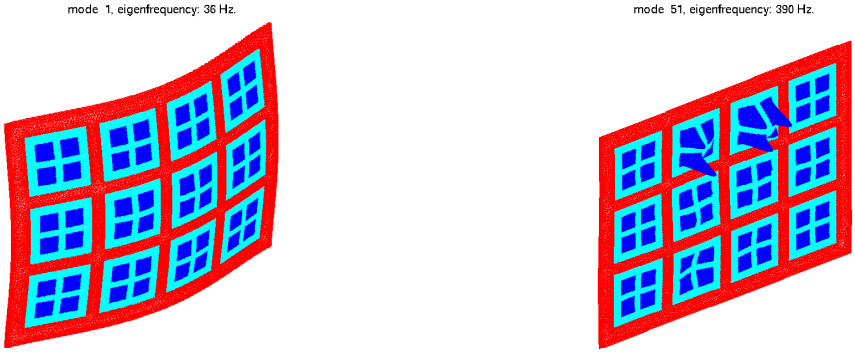

Figure 3: First elastic mode (left), 51st elastic mode (right)

The first elastic mode (occuring at $f_1 = \omega_1/(2\pi) = 36Hz$) is a global one while the 51st and the 215th elastic modes are local ones respectively corresponding to displacements of the $\mathcal{M}$ and $\mathcal{H}$ scales (with $f_{51} = 390Hz$ and $f_{215} = 936Hz$). The 50th elastic mode presents displacements of all the three scales ($f_{50} = 380Hz$). Most of the elastic modes are, in this same way, constituted of displacements of several scales.

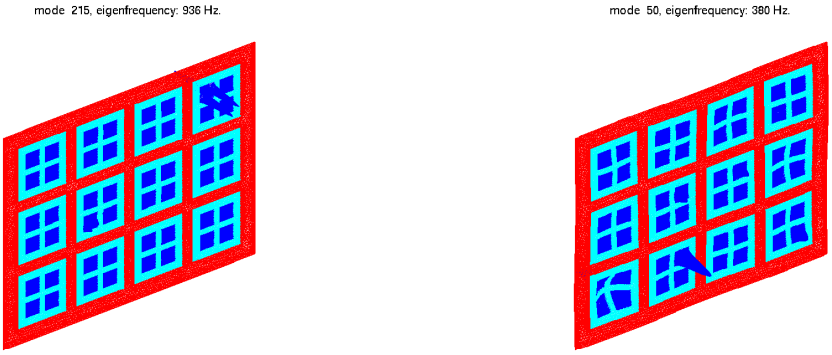

Figure 4: 215th elastic mode (left), 50th elastic mode (right)

6.2.2 $\mathcal{S}$-scale elastic modes

We aim to construct the three admissible displacements subspaces $\mathbb{V}_{\mathcal{L}}$, $\mathbb{V}_{\mathcal{M}}$, and $\mathbb{V}_{\mathcal{H}}$ associated with the three scales $\mathcal{L}$, $\mathcal{M}$, and $\mathcal{H}$ that respectively correspond to the stiff master structure, to the flexible panels, and to the high-flexible sub-panels. Their construction entirely relies on the definition of the displacements spaces $\mathbb{H}^1_r$ and $\mathbb{H}^2_r$. A first step consists in uniformly partitionning the domain of the structure into 20 subdomains (these subdomains do not coincide with the different panels, see Fig. 5). Space $\mathbb{H}^1_r$ is then defined as the set of vectors whose translation components vary, in each subdomain, as linear functions (in the present case, they correspond to rigid body displacements) whereas their rotation components are set to zero. This reduced kinematics for each subdomain allows the filtering of small-wavelength displacements associated with the panels and sub-panels ($\mathcal{M}$ and $\mathcal{H}$ scales) to be performed. Similarly, space $\mathbb{H}^2_r$ is constructed such that the displacements associated with the sub-panels only (scale $\mathcal{H}$) are filtered. It is then defined as the set of vectors whose translation components vary, in each subdomain, as polynomials of degree 3 whereas their rotation components are set to zero. This more precise kinematics ($\mathbb{H}^2_r \supset \mathbb{H}^1_r$) is such that displacements of scale $\mathcal{M}$ are preserved while those of scale $\mathcal{H}$ are still filtered. For spaces $\mathbb{H}^1_r$ and $\mathbb{H}^2_r$, the degrees of the polynomials are defined such that they roughly satisfy these conditions.

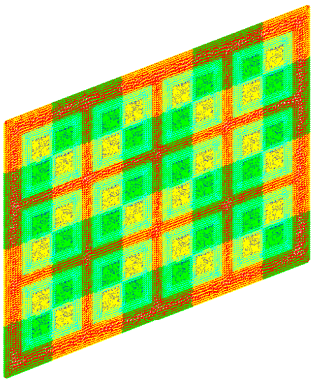

Figure 5: Subdomains

The projection matrices $[H^{\mathcal{L}}]$, $[H^{\mathcal{M}}]$, and $[H^{\mathcal{H}}]$ of ranks $d_{\mathcal{L}} = 60$, $d_{\mathcal{M}} = 200 - 60$, and $d_{\mathcal{H}} = m - 200$ are constructed accordingly to the subspaces $\mathbb{H}_{\mathcal{L}} = \mathbb{H}^1_r$, $\mathbb{H}_{\mathcal{M}} = \mathbb{H}^2_r \cap \mathbb{H}^1_c$, and $\mathbb{H}_{\mathcal{H}} = \mathbb{H}^2_c$ of $\mathbb{R}^m$ and allow the three modified generalized eigenvalue problems defined in Eq. 6 to be constructed. The $\mathcal{L}$-, $\mathcal{M}$-, and $\mathcal{H}$-scale elastic modes are obtained using Eq. (8) and respectively belong to the subspaces $\mathbb{V}^{(n_{\mathcal{L}})}_{\mathcal{L}}$, $\mathbb{V}^{(n_{\mathcal{M}})}_{\mathcal{M}}$, and $\mathbb{V}^{(n_{\mathcal{H}})}_{\mathcal{H}}$ with $n_{\mathcal{L}} = 60 \leq d_{\mathcal{L}}$, $n_{\mathcal{M}} = 125 \leq d_{\mathcal{M}}$, and $n_{\mathcal{H}} = 454 \leq d_{\mathcal{H}}$. In frequency band of analysis $\mathcal{B}$, there are 60 $\mathcal{L}$-scale elastic modes, 113 $\mathcal{M}$-scale elastic modes, and 367 $\mathcal{H}$-scale elastic modes. The modal densities of such $\mathcal{S}$-scale elastic modes are plotted in Fig. 6.

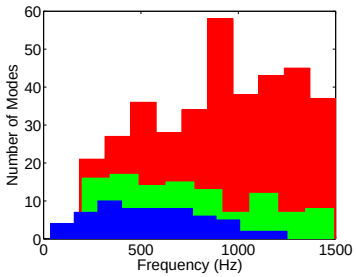

Figure 6: Modal densities: $\mathcal{L}$-scale elastic modes (blue or dark grey in b&w), $\mathcal{M}$-scale elastic modes (green or light grey in b&w), and $\mathcal{H}$-scale elastic modes (red or grey in b&w).

6.2.3 Frequency response functions

For all ω in $\mathcal{B}$, the structure is subjected to an external point load of $1N$ (following the normal direction) located in the master structure at the black-marked node depicted in Fig. 1. The generalized damping matrices are constructed using a modal damping model associated with a damping rate $\xi(\omega) = \xi_0\,\omega^{-\alpha}$ where ξ_0 and α are such that $\xi(\omega_1) = 0.04$ and $\xi(\omega_{500}) = 0.01$ with $f_1 = \omega_1/(2\pi) = 36Hz$ and $f_{500} = \omega_{500}/(2\pi) = 1721Hz$. The modulus in log-scale and the unwrapped phase angle of the normal displacement of the observation node (located in the master structure at the white-marked point depicted in Fig. 1), are calculated using the reduced-order model (ROM) constructed with the elastic-modes projection basis with convergence reached in $\mathcal{B}$ ($n = 500$), and are plotted in Fig. 7 and 8.

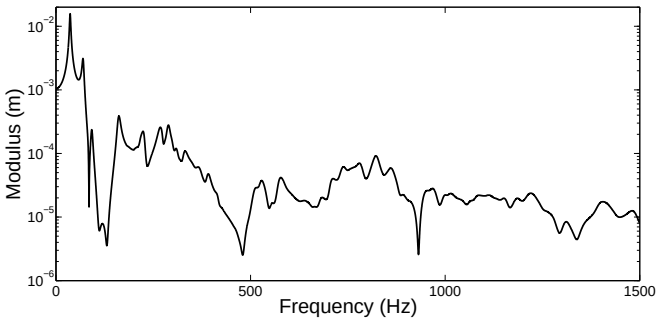

Figure 7: Modulus in log-scale using the ROM (converged, with $n = 500$)

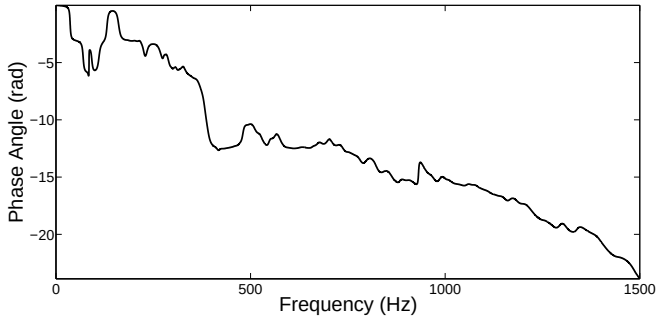

Figure 8: Phase angle using the ROM (converged, with $n = 500$)

The analysis of the modulus and of the phase (see Fig. 7 and 8) joined to the analysis of the modal density (see Fig. 2) lead us to define the three frequency bands as $]0, 200]Hz$ for LF, $]200, 1000]Hz$ for MF, and $]1000, 1500]Hz$ for HF.

Nominal reduced-order models For the different approximations $\mathbb{U}_{n_\mathcal{L},n_\mathcal{M},n_\mathcal{H}}(\omega)$ with $\{\, n_\mathcal{L} = 60,\, n_\mathcal{M} = 0,\, n_\mathcal{H} = 0 \,\}$ ($\mathcal{L}$-scale ROM), $\{\, n_\mathcal{L} = 0,\, n_\mathcal{M} = 125,\, n_\mathcal{H} = 0 \,\}$ ($\mathcal{M}$-scale ROM), and $\{\, n_\mathcal{L} = 0,\, n_\mathcal{M} = 0,\, n_\mathcal{H} = 454 \,\}$ ($\mathcal{H}$-scale ROM) , the deterministic responses obtained from the nominal reduced-order models defined in Section 5.1 are plotted in Fig. 9.

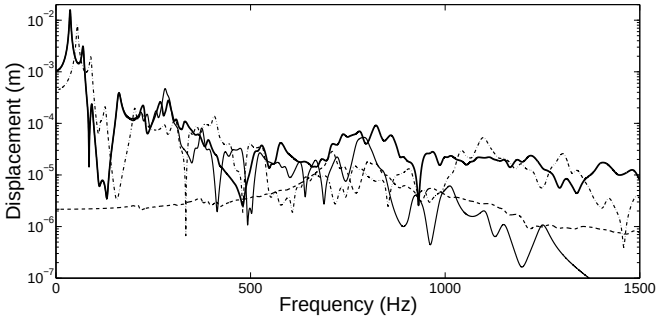

Figure 9: Modulus in log-scale using the ROM (converged reference, $n = 500$), solid thick line; using the $\mathcal{L}$-scale ROM ($n_{\mathcal{L}} = 60$), solid thin line; using the $\mathcal{M}$-scale ROM ($n_{\mathcal{M}} = 125$), mixed thin line; using the $\mathcal{H}$-scale ROM ($n_{\mathcal{H}} = 454$), dashed thin line.

The $\mathcal{L}$-scale ROM is accurate in the low-frequency band but rapidly loses fidelity thereafter. There is a large difference in the high-frequency band. The $\mathcal{M}$- and $\mathcal{H}$-scales ROM are not accurate anywhere in the frequency band since the response is never solely driven by one of these two scales.

The deterministic responses associated with the nominal reduced-order models defined in Section 5.1 for the different approximations $\mathbb{U}_{n_{\mathcal{L}},n_{\mathcal{M}},n_{\mathcal{H}}}(\omega)$ with $\{\, n_{\mathcal{L}} = 60,\, n_{\mathcal{M}} = 0,\, n_{\mathcal{H}} = 0 \,\}$ ($\mathcal{L}$-scale ROM), $\{\, n_{\mathcal{L}} = 60,\, n_{\mathcal{M}} = 125,\, n_{\mathcal{H}} = 0 \,\}$ ($\mathcal{L} \cup \mathcal{M}$-scales ROM), and $\{\, n_{\mathcal{L}} = 60,\, n_{\mathcal{M}} = 125,\, n_{\mathcal{H}} = 454 \,\}$ ($\mathcal{L} \cup \mathcal{M} \cup \mathcal{H}$-scales ROM) are plotted in Fig. 10.

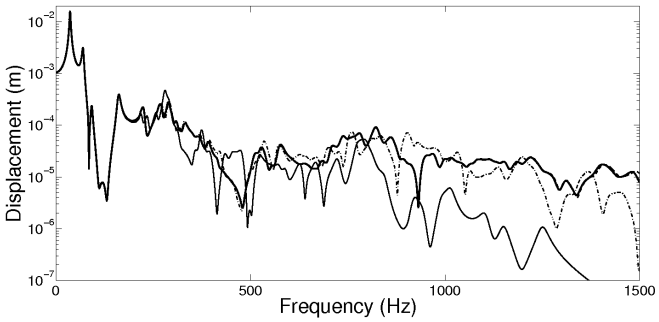

Figure 10: Modulus in log-scale using the ROM (converged reference, $n = 500$), solid thick line; using the $\mathcal{L}$-scale ROM ($n_{\mathcal{L}} = 60$), solid thin line; using the $\mathcal{L} \cup \mathcal{M}$-scales ROM ($n_{\mathcal{L}} + n_{\mathcal{M}} = 185$), mixed thin line; using the $\mathcal{L} \cup \mathcal{M} \cup \mathcal{H}$-scales ROM ($n_{\mathcal{L}} + n_{\mathcal{M}} + n_{\mathcal{H}} = 639$), dashed thin line.

The response obtained using the $\mathcal{L} \cup \mathcal{M} \cup \mathcal{H}$-scales ROM is superimposed on the reference. The response obtained using the $\mathcal{L} \cup \mathcal{M}$-scales ROM is superimposed on the reference up to $500Hz$ but progressively loses accuracy in higher frequencies. It should be noted that the reference (exact) response associated with the ROM does not take into account the fluctuations due to the real system variabilities and due to uncertainties in the computational model. It can be seen that, the prediction given by the $\mathcal{L} \cup \mathcal{M}$-scales ROM is good enough in all the frequency band with respect to the prediction given by the ROM.

Stochastic reduced-order models The random responses $\mathbf{U}_{n_{\mathcal{L}},n_{\mathcal{M}},n_{\mathcal{H}}}(\omega)$ with $n_{\mathcal{L}} = 60$, $n_{\mathcal{M}} = 125$, and $n_{\mathcal{H}} = 454$ obtained from the stochastic reduced-order models defined in Section 5.2.3 using 1000 realizations of the Monte-Carlo simulation method, and constructed using different combinations for the values of the hyperparameters are plotted: in Fig. 11 for the first combination (SROM$_1$), in Fig. 12 for the second combination (SROM$_2$), and in Fig. 13 for the third combination (SROM$_3$). The confidence regions correspond to a probability level $P_c = 0.95$. The three different combinations for the values of the hyperparameters are the following:

- $\delta_{\mathcal{L}}^{\mathbf{M}} = \delta_{\mathcal{L}}^{\mathbf{K}} = 0.2, \quad \delta_{\mathcal{M}}^{\mathbf{M}} = \delta_{\mathcal{M}}^{\mathbf{K}} = 0, \quad \delta_{\mathcal{H}}^{\mathbf{M}} = \delta_{\mathcal{H}}^{\mathbf{K}} = 0, \quad$ and $\quad \delta_{\mathcal{L}}^{\mathbf{D}} = \delta_{\mathcal{M}}^{\mathbf{D}} = \delta_{\mathcal{H}}^{\mathbf{D}} = 0.$
- $\delta_{\mathcal{L}}^{\mathbf{M}} = \delta_{\mathcal{L}}^{\mathbf{K}} = 0, \quad \delta_{\mathcal{M}}^{\mathbf{M}} = \delta_{\mathcal{M}}^{\mathbf{K}} = 0.2, \quad \delta_{\mathcal{H}}^{\mathbf{M}} = \delta_{\mathcal{H}}^{\mathbf{K}} = 0, \quad$ and $\quad \delta_{\mathcal{L}}^{\mathbf{D}} = \delta_{\mathcal{M}}^{\mathbf{D}} = \delta_{\mathcal{H}}^{\mathbf{D}} = 0.$
- $\delta_{\mathcal{L}}^{\mathbf{M}} = \delta_{\mathcal{L}}^{\mathbf{K}} = 0, \quad \delta_{\mathcal{M}}^{\mathbf{M}} = \delta_{\mathcal{M}}^{\mathbf{K}} = 0, \quad \delta_{\mathcal{H}}^{\mathbf{M}} = \delta_{\mathcal{H}}^{\mathbf{K}} = 0.2, \quad$ and $\quad \delta_{\mathcal{L}}^{\mathbf{D}} = \delta_{\mathcal{M}}^{\mathbf{D}} = \delta_{\mathcal{H}}^{\mathbf{D}} = 0.$

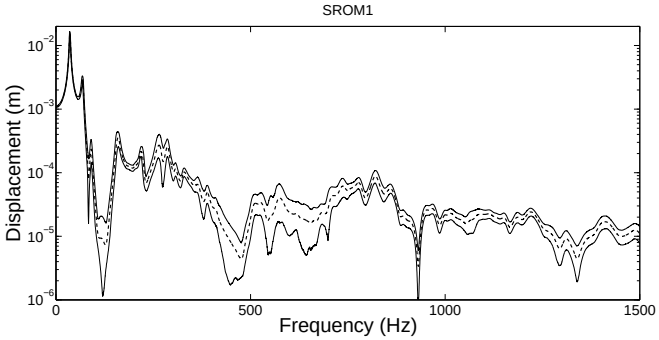

Figure 11: Random frequency response in log-scale using SROM_1: upper and lower bounds of the confidence region, solid lines; mean response, dashed line.

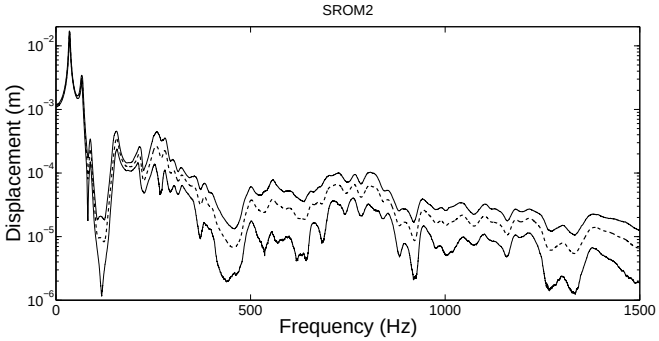

Figure 12: Random frequency response in log-scale using SROM_2: upper and lower bounds of the confidence region, solid lines; mean response, dashed line.

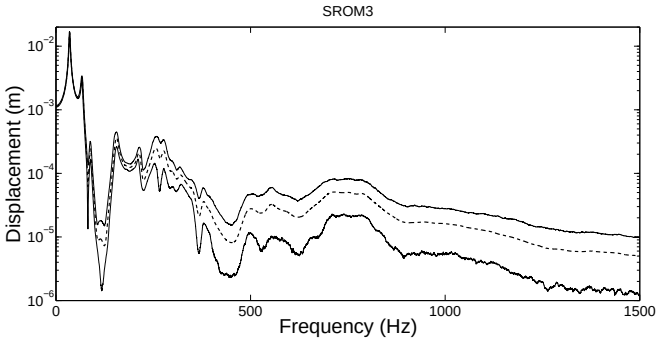

Figure 13: Random frequency response in log-scale using SROM_3: upper and lower bounds of the confidence region, solid lines; mean response, dashed line.

In Fig. 11, it can be seen that the level of uncertainties, which is confered to the $\mathcal{L}$-scale, results in a dispersion for the global level of the response while its fluctuations remain with respect to the frequency. In contrast, Fig. 13 shows that the frequency fluctuations of the random response obtained using SROM_3, for which uncertainties are taken into account only for the $\mathcal{H}$-scale, are diminished, especially in the high-frequency

band. Moreover, compared to the random response obtained using SROM_1, the widths of the confidence regions obtained using SROM_2 and SROM_3 are larger in the MF and HF bands, while it is not the case in the LF band.

7 Conclusions

In this paper, we have presented a general methodology, for constructing a frequency-multiscale representation of the admissible displacements space in the framework of computational structural dynamics. Such a representation allows us to construct an adapted nonparametric probabilistic model of uncertainties for each frequency-scale (LF, MF, and HF). The methodology proposed has been validated on a simple structure which is representative of complex structures exhibiting LF, MF, and HF behaviors. The validation on a complex industrial structure is in progress.

References

[1] Ohayon, R. and Soize, C., *Structural acoustics and vibration*, Academic Press (1998).

[2] Argyris, J. and Mlejnek, H. P., *Dynamics of Structures*, North-Holland, Amsterdam (1991).

[3] R. Lyon, G. Maidanik, *Statistical methods in vibration analysis*, AIAA Journal, 2(6), 1015-1024, 1964.

[4] R. H. Lyon, R.G. DeJong, *Theory and Application of Statistical Energy Analysis*, Butterworths-Heimann, Boston, MA, 1995.

[5] Ibrahim, R. A., *Parametric Random Vibration*, John Wiley and Sons, New York, 1985.

[6] Ghanem, R. G. and Spanos, P. D., *Stochastic Finite Elements: A Spectral Approach*, Springer-Verlag, New York, 1991.

[7] C. Soize, *A nonparametric model of random uncertainties for reduced matrix models in structural dynamics*, Probabilistic Engineering Mechanics 15(3) (2000) 277-294.

[8] C. Soize, *Generalized probabilistic approach of uncertainties in computational dynamics using random matrices and polynomial chaos decomposition*, International Journal for Numerical Methods in Engineering 81 (8) (2010) 1939-1970.

[9] Soize, C. and Batou, A., *Stochastic reduced-order model in low-frequency dynamics in presence of numerous local elastic modes*, Journal of applied mechanics - Transactions of the ASME, 78(6):061003, 2011.

[10] A. Batou, C. Soize, *Uncertainty quantification in low-frequency dynamics of complex beam-like structures having a high-modal density*, International Journal for Uncertainty Quantification, 1(1), 431-451, 2013.

[11] Zienkiewicz, O. C., and Taylor, R. L., *The Finite Element Method*, 5th ed., Butterworth-Heinemann, Oxford, 2000.

[12] Bathe, K. J. and Wilson, E. L., *Numerical Methods in the Finite Element Method*, Prentice-Hall, Englewood Cliffs, NJ, 1976.

[13] Shannon, C. E., *A Mathematical Theory of Communication*, Bell Syst. Tech. J., 27, pp. 379423 and pp. 623659, 1948.

[14] Jaynes, E. T., *Information Theory and Statistical Mechanics*, Phys. Rev., 106(4), pp. 620630 and 108(2), pp. 171190, 1957.

[15] Rubinstein, R., *Simulation and the Monte Carlo Method*, John Wiley and Sons, 1980.